Available online at www.sciencedirect.com
ScienceDirect
Ceramics International 33 (2007) 1237–1241
CERAMICS INTERNATIONAL
www.elsevier.com/locate/ceramint

Synthesis and electrical properties of $Ln_{0.6}Ca_{0.4}FeO_{3-\delta}$ (Ln=Pr, Nd, Sm) as cathode materials for IT-SOFC

Yong-hong Chen [a,b,*], Yi-jun Wei [a], Hong-hai Zhong [b], Jian-feng Gao [b], Xing-qin Liu [b], Guang-yao Meng [b]

[a] Center of Experiment and Communication, Huainan Normal University, Huainan 232001, PR China
[b] Department of Materials Science and Engineering, University of Science and Technology of China, Hefei 230026, PR China

Received 1 August 2005; received in revised form 28 February 2006; accepted 29 March 2006
Available online 1 September 2006

Abstract

Fine powders of $Ln_{0.6}Ca_{0.4}FeO_{3-\delta}$ (Ln=Pr, Nd, Sm) were prepared by a glycine-nitrate process (GNP). The preparation process, thermal properties, phase constituents, and microstructure of the samples were characterized by FT-IR, TG-DSC, XRD and TEM, respectively. The results show that all of the powders have perovskite-type structure with orthorhombic symmetry and mean particle size of 25 nm. The relative density of $Pr_{0.6}Ca_{0.4}FeO_{3-\delta}$ and $Nd_{0.6}Ca_{0.4}FeO_{3-\delta}$ decreased with sintering temperature, while increased for $Sm_{0.6}Ca_{0.4}FeO_{3-\delta}$. The DC four-probe measurement indicated that both $Pr_{0.6}Ca_{0.4}FeO_{3-\delta}$ and $Nd_{0.6}Ca_{0.4}FeO_{3-\delta}$ exhibit fairly high electrical conductivity, over 100 S cm^{-1} at $T > 650$ °C, high enough for application as cathode materials for IT-SOFC. The temperature dependence of the conductivity for $Nd_{0.6}Ca_{0.4}FeO_{3-\delta}$ d consists of two straight lines with activation energies of 160.2 and 18.6 kJ mol^{-1}, respectively, for the sample sintered at 1100 °C for 2 h. The conduction mechanism of the materials is discussed in terms of non-stoichiometry.

Keywords: A. Sintering; B. Microstructure; C. Electrical conductivity; D. Perovskites

1. Introduction

Solid oxide fuel cells (SOFC) are considered as one of the most promising energy conversion devices that exhibit advantages such as high efficiency, system compactness and low environmental pollution [1,2]. The traditional SOFC operated at high temperature up to 1000 °C presents some problems related to the cost of the materials and fabrication [3], which hinder its commercialization. Therefore, a common trend is to develop reduced temperature SOFC systems which can be operated at lower temperature, typically below 750 °C. So intermediate-temperature solid oxide fuel cells (IT-SOFC) have attracted much attention in recent years [4–6]. With the reduction of operating temperature, however, the polarization processes at the cathode limit SOFC performance [7]. Indeed, the polarization loss of the cathode exceeds 65% of the total voltage loss in the SOFC [8]. Accordingly, much work has been recently carried out to search for high performance cathode materials for IT-SOFC [9–11].

The function of SOFC cathodes is to adsorb and catalyse oxygen so as to produce oxygen ions, and transfer them to the interface with the electrolyte. These materials should possess fast oxide ion transport in addition to high electrical conductivity. It has been found that some perovskite-type (ABO_3) rare-earth complex oxides exhibit mixed oxygen ionic and electrical conductivities, and for this reason they are widely studied for application in SOFC. Among these materials, $La_{1-x}Sr_xMnO_{3-\delta}$ has been used as cathode material for traditional SOFC, because it presents favourable electrochemical characteristics at high temperature, but it is not suitable for IT-SOFC [7]. The lanthanum–strontium ferrites complex oxides such as $(La_{0.8}Sr_{0.2})_xFeO_{3-\delta}$ (LSF) have been used as a cathode for IT-SOFC [6,12,13]. The thermal expansion coefficient of LSF is similar with that of the electrolyte, the long-term stability is well known, and the catalytic activity for oxygen reduction is also favourable. Calcium is another

* Corresponding author at: Center of Experiment and Communication, Huainan Normal University, Huainan 232001, PR China.
Tel.: +86 554 6643603; fax: +86 554 6672451.
E-mail address: chenyh@hnnu.edu.cn (Y.-h. Chen).

0272-8842/$32.00
doi:10.1016/j.ceramint.2006.03.035

effective doping-element at the A-site of ABO_3, with less cost. Praseodymium, Neodymium and Samarium are the same as light rare earths. In this study, three samples of $Ln_{0.6}Ca_{0.4}FeO_{3-\delta}$ (Ln=Pr, Nd and Sm, labeled as PCF, NCF, and SCF, respectively) with the perovskite structure were prepared by the glycine-nitrate process (GNP). Their chemical composition, thermal stability and crystalline structure were investigated. The sintering activity and electrical conductivity of the powders obtained were also investigated.

2. Experimental procedure

2.1. Powders synthesis

All powders were synthesized by the GNP method [14]. The starting materials were $Pr(NO_3)_3{\cdot}6H_2O$, $Nd(NO_3)_3{\cdot}5H_2O$, $Sm(NO_3)_3{\cdot}6H_2O$, $Ca(NO_3)_2{\cdot}4H_2O$, $Fe(NO_3)_3{\cdot}9H_2O$ and glycine, all agents are of analytical grade. Nitrates were dissolved in de-ionized water with concentration of each solution ca. 1 mol L^{-1}, and then determined accurately by EDTA titration. A specific GNP process was used to produce powder from stoichiometric volumes of nitrate solution that were mixed in an evaporating pot with 1 mol of glycine added for each mole of total-metal ions. The mixture was stirred substantially and then heated on an electric stove to evaporate the solvent. After spontaneous combustion, the resultant iron oxide red ash was collected (named as primary powder), and calcined in static air at 850 °C for 2 h to remove any carbon residue; the product was named as calcined powder. All powders were ball-milled for 2 h to break down aggregates.

2.2. Characterization

Infrared spectra of coordinating solutions, primary powders and calcined powders were carried out on AVATAR 360 Fourier Transform Infrared Spectrometer (FT-IR). The phases of samples were identified by X-ray diffraction (XRD) using a PHILIPS X′ Pert Pro Super diffractometer. Simultaneous differential scanning calorimetry and thermogravimeter analysis (DSC-TG) of the primary powders were conducted on a SDT 2960 thermal analyser. Microstructure of the powders was observed by transmission electron microscopy (TEM) using a HITACHI 600 electron microscope.

2.3. Sintering and electrical conductivity testing

The calcined powders were uniaxially die-pressed at 200 MPa into two different shapes. One was a wafer 13 mm diameter and about 1–2 mm thickness, which was then sintered in a programmable furnace in static air with a heating rate of 1–2 °C min^{-1} in the temperature range from 1000 to 1400 °C for 2 h. The other was a 40 × 6 × 2 mm^3 bar, which was prepared for electrical conductivity measurement after sintering 1100–1300 °C in air. The relative densities of sintered specimens were determined by the Archimedes method. The electrical conductivity of sintered bars was measured in air from 450 to 800 °C at 50 °C intervals by a DC four-probe technique with GDM 8055G digital multimeter.

3. Results and discussion

3.1. FT-IR analysis of the as-obtained powders

The glycine-nitrate process is a self-sustaining gel-combustion synthesis technique. Aqueous precursor solutions containing metal nitrates and glycine are heated until they auto-ignite. Glycine serves a dual role: in the precursor solution, glycine complexes the metal cations, thereby preventing selective precipitation and upon ignition, glycine is oxidized by the nitrate ions, thereby serving as the fuel for the combustion reaction. Fig. 1 shows the FT-IR spectra of the glycine, precursor solution, primary powder and calcined powder heated at 850 °C for 2 h for $Nd_{0.6}Ca_{0.4}FeO_{3-\delta}$, respectively. The absorptive peaks of glycine at 2600–3200 cm^{-1} are characteristic bands of O–H and N–H groups, while the peak at 1597 cm^{-1} is the carboxyl group (Fig. 1(a)). In the spectra of precursor solution (Fig. 1(b)), there are two typical absorptive bands at 1648 cm^{-1} and 1365 cm^{-1}, corresponding to water and nitrate (NO_3^-) absorption, respectively. Comparing Fig. 1(a) with Fig. 1(b), we can see that the characteristic bands of O–H and N–H groups in solution disappeared, indicating the coordinate bond between glycine and metal ions to form. Primary powder presented the nitrate absorption peak in the range 1382–1426 cm^{-1} and the carbonate peak at 1599 cm^{-1}. Meanwhile, the stretching vibration at 575 cm^{-1} and deformation vibration at 414 cm^{-1} of B–O bond for ABO_3 perovskite-type may be observed (Fig. 1(c)). After calcining at 850 °C for 2 h, the intensity of nitrate and carbonate peaks

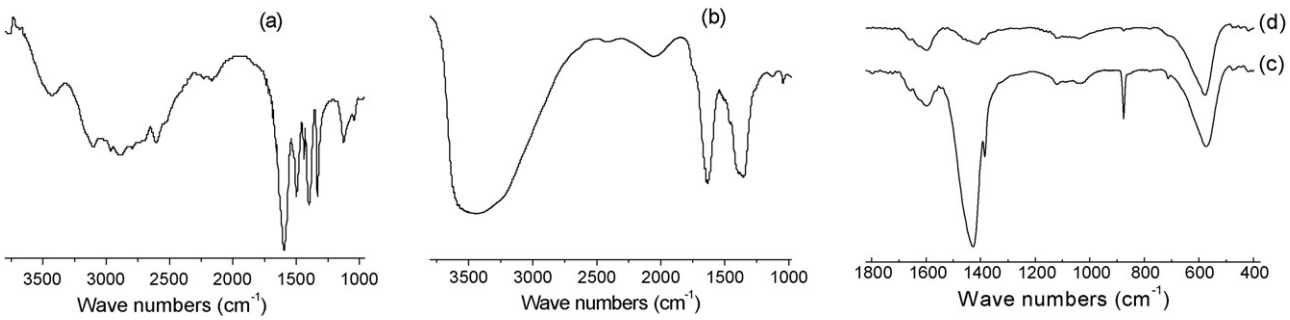

Fig. 1. FT-IR spectra of (a) glycine, (b) precursor solution, (c) primary powder, and (d) calcined powder at 850 °C for 2 h.

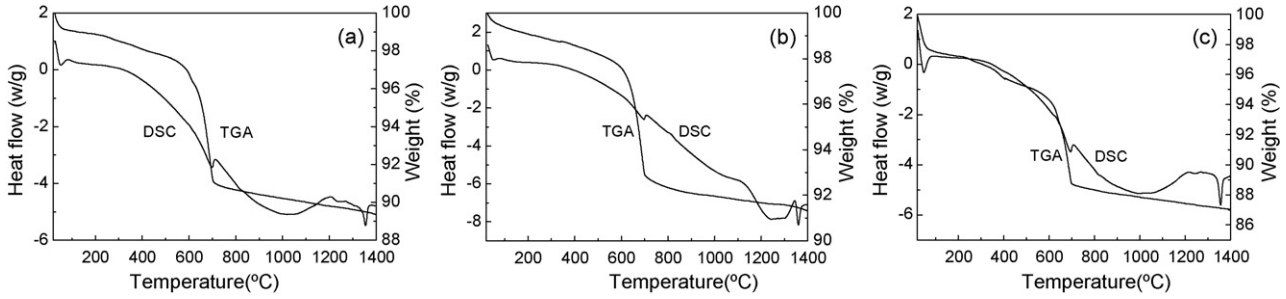

Fig. 2. TG-DSC curves of the primary powders for (a) PCF, (b) NCF, and (c) SCF.

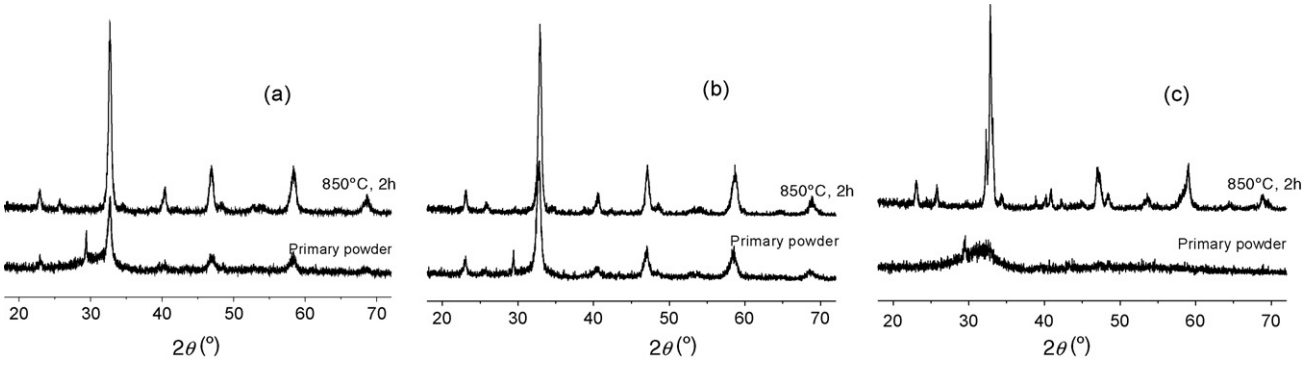

Fig. 3. X-ray diffraction patterns of (a) PCF, (b) NCF, and (c) SCF.

decreased (Fig. 1(d)). This result is consistent with the pattern of XRD. The FT-IR spectra of other samples were similar to the ones described above.

3.2. TG-DSC analysis

TG-DSC was used to analyze the formation process of the product and phase stability. Fig. 2(a)–(c) shows the dependence on temperature of the heat-flow and weight for the primary powders of PCF, NCF, and SCF, respectively. It is easily seen that the TG curves of the three samples are quite similar. At $T < 600$ °C, both of the PCF and NCF have ca. 2 wt.% and SCF has ca. 4 wt.% weight loss caused by the removal of remnant water. There was only one abrupt weight loss that occurred at 600–700 °C. Correspondingly, the DSC plots show slightly endothermic peaks. Correlated with the results of the X-ray diffraction, it is assumed that the weight loss was caused by the decomposition of the calcium carbonate remained in the products. At $T > 700$ °C, the weight loss slightly corresponded with the partial loss of the lattice oxygen [13]. Meanwhile, the DSC curves of the three samples revealed two endothermic processes at high temperature, but no associated mass loss on the TG curves. This can be ascribed to a crystalline phase change that may result from the melting process of ferrites at high temperature.

3.3. Structure characteristics

Fig. 3(a)–(c) shows the X-ray diffraction patterns of PCF, NCF, and SCF, respectively, with the primary powders spectra located on the bottom. A perovskite-type crystalline phase has been formed in PCF and NCF powders (Fig. 3(a) and (b), JCPDF card No. 74-2203) nearly at the start of ignition, accompanied by minor amounts of $CaCO_3$ (JCPDF card No. 85-1108). In contrast, no peaks can be identified on SCF XRD patterns (Fig. 3(c)), which implies that the SCF primary powder is amorphous. The XRD patterns of the three powders calcined at 850 °C for 2 h present sharp reflections, showing that the materials are well crystallized after heat treatment. The structure agrees with $LaFeO_3$, of cubic perovskite structure [15]. Note that the size of particles increased after calcination. These results agree with the literature [14].

Fig. 4 shows a TEM micrograph of the PCF powder whose particles show approx globular shapes with average size of ca.

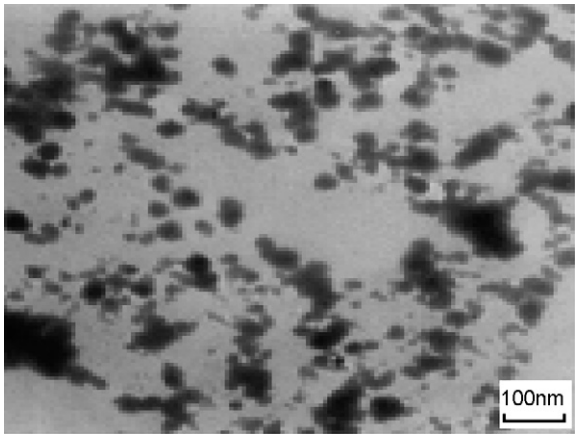

Fig. 4. TEM micrograph of the PCF powder.

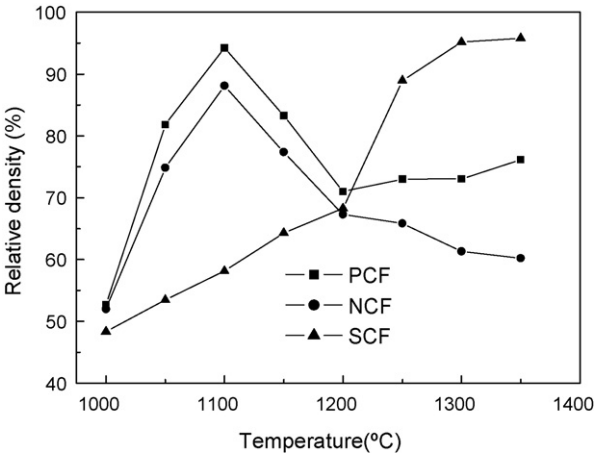

Fig. 5. Relative density of specimen vs. sintering temperature.

25 nm, and only slightly agglomerated. NCF and SCF morphologies are similar to PCF.

3.4. Sinterability

Sinterability is one of the most important properties for the SOFC cathode materials, with direct influence on the fabrication of the electrode and the stability of the cell. Fig. 5 shows the relative density as a function of sintering temperature for the three specimens. The relative density of PCF and NCF increased with the sintering temperature up to 1100 °C, and then decreased. At 1100 °C, the relative density of PCF and NCF is the largest over all the temperatures studied, i.e. 94.2% and 88.1%, respectively. In contrast, the relative density of SCF increased with sintering temperature up to reach 95.14% at 1300 °C. The decrease of relative density with sintering temperature for PCF and NCF at $T > 1100$ °C may derive from the phase change taking place at higher temperature, just as shown in TG-DSC curves.

Shown in Fig. 6 is the dependence of sintering temperature on specimens shrinkage. The linear shrinkage of specimens for PCF and NCF sintering at 1100 °C for 2 h is 19.84% and 19.23%, respectively, while for SCF is 2.99% only.

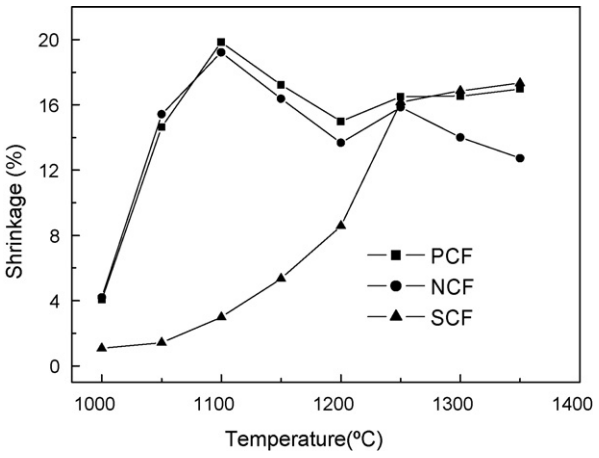

Fig. 6. Shrinkage of specimen vs. sintering temperature.

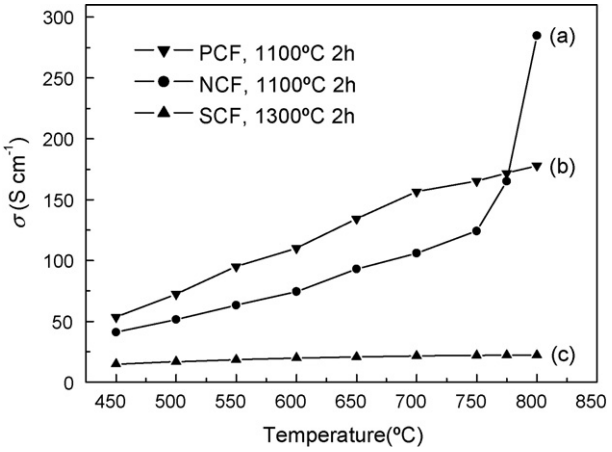

Fig. 7. Electrical conductivity of specimens at different temperature in air. The specimens for the cathodes were (a) NCF sintered at 1100 °C for 2 h, (b) PCF sintered at 1100 °C for 2 h, and (c) SCF sintered at 1300 °C for 2 h, respectively.

3.5. Electrical conductivity

Fig. 7 presents the electrical conductivity of the specimens against temperature measured in air at 450–800 °C. The conductivity of PCF and NCF is larger than for SCF. At $T < 750$ °C, the electrical conductivity of both PCF and NCF materials increases linearly with temperature, while the SCF is nearly independent on temperature. At 750 °C, the slope of NCF turns sharply, which may indicate that the mechanism for electrical conduction changes at higher temperature. It is important to note that the electrical conductivity of PCF and NCF is 284.8 and 177.98 S cm^{-1} at 800 °C, respectively, well over 100 S cm^{-1}, i.e. the general requirement for electrode materials in IT-SOFC. This implies that the partial substitution of Ca^{2+} ion in the A-site for $PrFeO_3$ and $NdFeO_3$ has an advantageous effect on its electrical conductivity, and may have potential application for IT-SOFC cathode materials.

Plots of $\ln(\sigma T)$ versus 1000 T^{-1} is PCF and SCF (Fig. 8), it shows that over the temperature range studied, $\ln(\sigma T)$ decreases linearly as 1000 T^{-1} increases, which agree with the Arrhenius equation, and implies that the electrical conduction agrees with

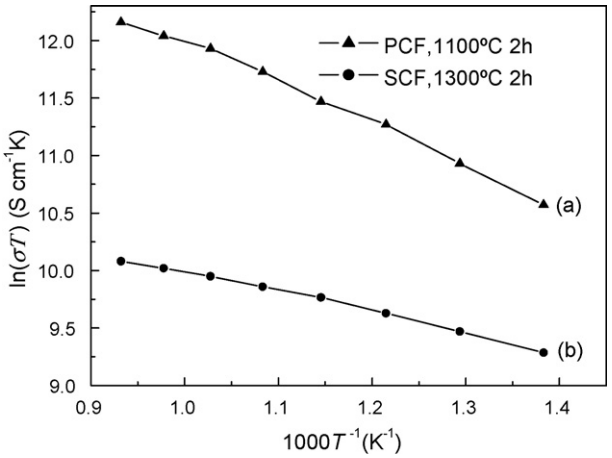

Fig. 8. Arrhenius plots of samples with (a) PCF sintered at 1100 °C for 2 h and (b) SCF sintered at 1300 °C for 2 h, respectively.

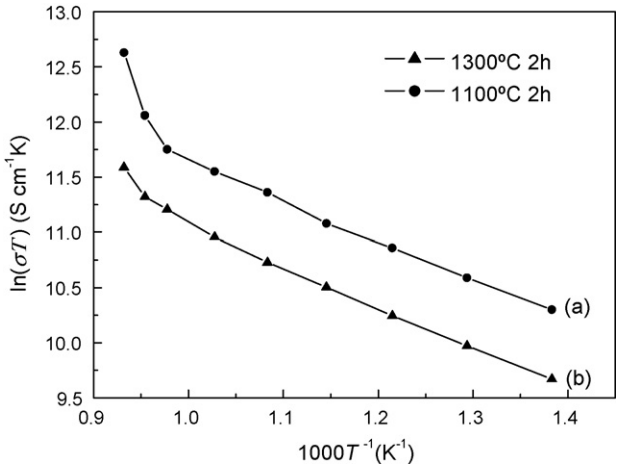

Fig. 9. Arrhenius conductivity plots for NCF with (a) sintered at 1100 °C for 2 h and (b) sintered at 1300 °C for 2 h.

the small polarons mechanism [16]. From Fig. 8, it can be calculated that the electrical activation energy is 29.57 and 14.66 kJ mol^{-1}, for PCF and NCF, respectively.

Fig. 9 shows the Arrhenius plots of NCF sintered at 1100 °C (a) and 1300 °C (b) for 2 h. At $T < 750$ °C, the relationships between $\ln(\sigma T)$ and 1000 T^{-1} is linear and the curves of the two samples are nearly parallel, and the activation energy for electrical conduction is 18.6 and 19.4 kJ mol^{-1}, respectively. At $T > 750$ °C, both plots depart from the original track and become steeper. The electrical conductivity of samples sintered at 1100 °C is always larger than that sintered at 1300 °C.

4. Conclusions

1. Perovskite-type structure and nano-sized powders were obtained for $Ln_{0.6}Ca_{0.4}FeO_{3-\delta}$ (Ln=Pr, Nd, Sm) by the glycine-nitrate process method.
2. The relative density of PCF and NCF was 94.2% and 88.1% when sintered at 1100 °C for 2 h. That of SCF was only 58.4% for similar heat treatment.
3. At $T \leq 750$ °C, the electrical conductivity of both PCF and NCF materials increases linearly with temperature, while the electrical conductivity of SCF was independent of temperature. The hopping of small polarons has been regarded as the dominating mechanism for the electrical conduction at 450–750 °C.
4. At $T > 750$ °C, the Arrhenius curves of NCF increase sharply, which was considered to be the result of cooperating ionic and electronic conductivity.
5. The electrical conductivity of PCF and NCF samples was over 100 S cm^{-1} at $T \geq 650$ °C, indicating that they have potential application for IT-SOFC cathode materials.

Acknowledgements

One of the authors (Yong-hong Chen) is grateful to bureau education Anhui province of China for providing the financial support (2004kj326).

References

[1] S.P. Simner, J.P. Shelton, M.D. Anderson, J.W. Stevenson, Solid State Ionics 161 (2003) 11–18.
[2] T.A. Damberger, J. Power Sources 71 (1998) 45–50.
[3] H.Y. Tu, Y. Takeda, N. Imanishi, O. Yamamoto, Solid State Ionics 117 (1999) 277–281.
[4] R.N. Basu, F. Tietz, O. Teller, E. Wessel, J. Solid State Electrochem. 7 (2003) 416–420.
[5] M. Koyama, C.J. Wen, T. Masuyama, J. Otomo, H. Fukunaga, K. Yamada, K. Eguchi, H. takahashi, J. Electrochem. Soc. 148 (2001) A795–A801.
[6] S.P. Simner, J.E. Bonnett, N.L. Canfield, K.D. Meinhardt, J.P. Shelton, V.L. Sprenkle, J.W. Stevenson, J. Power Sources 113 (2003) 1–10.
[7] R. Doshi, V.L. Richards, J.D. Carter, X.P. Wang, K. Michael, J. Electrochem. Soc. 146 (1999) 1273–1278.
[8] M. Koyama, C.J. Wen, K. Yamada, J. Electrochem. Soc. 147 (2000) 87–91.
[9] D. Stöver, H.P. Buchkremer, S. Uhlenbruck, Ceram. Int. 30 (2004) 1107–1113.
[10] L.-W. Tai, M.M. Nasrallah, H.U. Anderson, J. Solid State Chem. 118 (1995) 117–124.
[11] W.H. Huang, J.H. Yang, H.W. Nie, Z.Y. Lu, H.Y. Tu, T.L. Wen, J. Inorg. Mater. 17 (2002) 679–684.
[12] J.E. Elshof, M.H.R. Lanklorst, H.J.M. Bouwmeester, J. Electrochem. Soc. 144 (1997) 1060–1067.
[13] J.E. Elshof, M.H.R. Lanklorst, H.J.M. Bouwmeester, Solid State Ionics 99 (1997) 15–22.
[14] A.S. Mukasyan, C. Costello, K.P. Sherlock, D. Lafarga, A. Varma, Separation Purif. Technol. 25 (2001) 117–126.
[15] E. Bontempi, C. Garzella, S. Valetti, L.E. Depero, J. Eur. Ceram. Soc. 23 (2003) 2135–2142.
[16] L.-W. Tai, M.M. Nasrallah, H.U. Anderson, D.W. Sparlin, S.R. Sehlin, Solid State Ionics 76 (1995) 273–283.